LETTER

doi:10.1038/nature11840

Generation of electron Airy beams

Noa Voloch-Bloch[1], Yossi Lereah[1], Yigal Lilach[1], Avraham Gover[1] & Ady Arie[1]

Within the framework of quantum mechanics, a unique particle wave packet exists[1] in the form of the Airy function[2,3]. Its counter-intuitive properties are revealed as it propagates in time or space: the quantum probability wave packet preserves its shape despite dispersion or diffraction and propagates along a parabolic caustic trajectory, even though no force is applied. This does not contradict Newton's laws of motion, because the wave packet centroid propagates along a straight line. Nearly 30 years later, this wave packet, known as an accelerating Airy beam, was realized[4] in the optical domain; later it was generalized to an orthogonal and complete family of beams[5] that propagate along parabolic trajectories, as well as to beams that propagate along arbitrary convex trajectories[6]. Here we report the experimental generation and observation of the Airy beams of free electrons. These electron Airy beams were generated by diffraction of electrons through a nanoscale hologram[7–9], which imprinted on the electrons' wavefunction a cubic phase modulation in the transverse plane. The highest-intensity lobes of the generated beams indeed followed parabolic trajectories. We directly observed a non-spreading electron wavefunction that self-heals[10], restoring its original shape after passing an obstacle. This holographic generation of electron Airy beams opens up new avenues for steering electronic wave packets like their photonic counterparts, because the wave packets can be imprinted with arbitrary shapes[5] or trajectories[6].

Curved light is an intriguing caustic phenomenon[2] common in nature and in everyday life; examples range from rainbows[3] to the bright light patterns that appear on the sea floor when sun shines on rippling water waves[2]. Caustics, already studied in the nineteenth century, led George Biddell Airy to discover the Airy function[3]. When the quantum mechanical probability density of a particle is imposed with the initial shape of an Airy function, the regions of maximum probability, that is, the intensity peaks of the Airy function, preserve their shape[11] and stay localized around parabolic trajectories in space, similar to that of a freely propagating projectile experiencing a transverse accelerating force. As already pointed out, this accelerating Airy wave packet[1] does not contradict Ehrenfest's theorem (embodying Newton's second law of motion), as the wave packet centroid travels along a straight path. The evolution of a light beam in space corresponds to the paraxial Helmholtz equation, which resembles the Schrödinger equation. This analogy led to the discovery and the experimental realization of the optical Airy beams[4]. The intriguing propagation dynamics of Airy beams is a caustic wave phenomenon that can be understood by ray analysis: the wave packet is composed of a family of rays that coalesce along a curved boundary[12]. The local angular momentum of Airy beams changes as they propagate, but the total momentum and energy are conserved[13]. Various applications followed the discovery of optical Airy beams, including microparticle manipulation[14], generation of plasma channels in air and water[15], surface Airy plasmons[16–18] and applications in lasers[19,20] and in nonlinear optics[21]. All of these rely on the Airy form of the wave packet of photons.

The spatial evolution of the envelope, Ψ, of an electron's wavefunction can be expressed using the paraxial Helmholtz equation (Supplementary Information, section 1):

$$\left(\nabla_{\perp}^2 + 2ik_{\mathrm{B}}\frac{\partial}{\partial z}\right)\Psi = 0$$

where $\nabla_{\perp}^2 = \partial^2/\partial x^2 + \partial^2/\partial y^2$ is the transverse derivative and $k_{\mathrm{B}} = p/\hbar = 2\pi/\lambda_{\mathrm{B}}$ is the de Broglie wavenumber of the electron ($\hbar$, Planck's constant divided by 2π). This equation has the same form as that of the Schrödinger equation. However, rather than describing the time evolution of the electron's wavefunction, it describes the wavefunction's evolution as it propagates in space. This is another manifestation of the analogy, widely used in optics, between beam diffraction in space and pulse dispersion in time. When the initial wavefunction of the electron is an Airy function (Ai), $\Psi(x,y,z=0) = \mathrm{Ai}(x/x_0)\mathrm{Ai}(y/y_0)$, where x_0 and y_0 are characteristic length scales, the general solution for the wave packet is[1,10,14]

$$\begin{aligned}\Psi(x,y,z) = {} & \mathrm{Ai}\left(\frac{x}{x_0} - \frac{z^2}{4k_{\mathrm{B}}^2 x_0^4}\right)\mathrm{Ai}\left(\frac{y}{y_0} - \frac{z^2}{4k_{\mathrm{B}}^2 y_0^4}\right) \\ & \times \exp\left(i\frac{xz}{2k_{\mathrm{B}}x_0^3} - i\frac{z^3}{12k_{\mathrm{B}}^3 x_0^6}\right) \\ & \times \exp\left(i\frac{yz}{2k_{\mathrm{B}}y_0^3} - i\frac{z^3}{12k_{\mathrm{B}}^3 y_0^6}\right)\end{aligned} \quad (1)$$

It is then clear from equation (1) that $|\Psi|^2$ preserves its shape and follows a parabolic trajectory. The parabolic trajectory is described by[22] $x(z) = z^2/4k_{\mathrm{B}}^2 x_0^3$, $y(z) = z^2/4k_{\mathrm{B}}^2 y_0^3$. The ideal Airy beam carries an infinite amount of energy, whereas in practice the Airy beam is truncated, having a finite energy. The finite Airy beam is obtained by multiplying the Airy function with an exponential or Gaussian window[4]. Nevertheless, over a finite distance, the finite Airy beam has all the special characteristics of the infinite Airy beam such as slow diffraction, curved trajectory and self-healing.

In optics, finite Airy beams were experimentally obtained by passing a Gaussian beam through a phase mask imprinting a cubic phase modulation in the transverse direction[4], and then doing an optical Fourier transform (the Fourier transform of a function having a cubic phase modulation results in an Airy function). Here we use electrons instead of photons. These electrons pass through a hologram that adds a transverse cubic phase, $\exp(i\varphi(x,y)) = \exp(ic_x x^3)\exp(ic_y y^3)$, to the wavefunction. Our hologram design method was to construct a binary diffraction grating with the following shape[23,24]:

$$h(x,y) = \frac{1}{2}h_0(\mathrm{sgn}\{\cos[2\pi x/\Lambda + c_x x^3 + c_y y^3] + D_{\mathrm{cycle}}\} + 1)$$

In this way, a cubic phase is imposed on a carrier frequency. The carrier period is Λ, h_0 is the ridge height of the binary phase mask and D_{cycle} is an arbitrary duty cycle factor. When electrons (or light) diffract from the binary structure, it decomposes into different diffraction orders; the complex amplitude of the mth-order diffracted beam is proportional to $\exp(im\phi(x,y))$. In the special case of a cubic phase modulation, each diffraction order is superimposed with a different cubic phase and so has an amplitude proportional to $\exp(im(c_x x^3 + c_y y^3))$. Each order therefore propagates along a different parabolic trajectory with a quadratic coefficient proportional to $1/m$ (Supplementary Information,

[1]Department of Physical Electronics, School of Electrical Engineering, Fleischman Faculty of Engineering, Tel Aviv University, Tel Aviv 69978, Israel.

section 2). We name this diffraction pattern the 'Airy lattice' (Figs 1 and 2). The general parametric equations of the trajectories of order m are

$$x_m(z) = -\frac{1}{m}\frac{1}{4k_B^2 x_0^3}z^2 + mz\frac{G}{k_B} + mf\frac{G}{k_B}$$
$$y_m(z) = \frac{1}{m}\frac{1}{4k_B^2 y_0^3}z^2 \quad (2)$$

where $G = 2\pi/\Lambda$ is the reciprocal lattice vector of the transmission hologram and f is the focal length of the lens. Note that the y trajectories include only a quadratic term, whereas the x trajectories contain both a quadratic term and a linear term, owing to the modulation of the carrier frequency. The Airy lattice is a novel type of lattice that diffracts but does not spread. Although each order diffracts in a different direction, each order stays localized and anomalously bends.

In our experiment, we use a field-emission-gun transmission electron microscope (FEG-TEM), operating at 200 keV. The de Broglie wavelength, including relativistic correction in this case, is approximately 2.5 pm. Therefore, to generate the inner structure of Airy beams as well as the spatial separation of different orders, we used nanoscale holograms (Supplementary Information, section 3). The micrographs of these nanoscale holograms are shown in Fig. 3b, c. The Fourier transform of the modulated wavefunction is done using a set of magnetic lenses, so that an electron Airy beam is obtained in the back focal plane of the FEG-TEM. This method is analogous to the method used to generate optical Airy beams[4], the only difference being that we manipulate electrons rather than photons. Some of the results from the Airy profiles are shown in Fig. 3d and Fig. 3e. Because the measurement plane is located at a fixed position in our FEG-TEM, we varied the focal lengths of the magnetic lenses to observe the formation and evolution of the electron Airy wave packet in space (Fig. 3a). The experiment details are given in Supplementary Information, section 4.

In the first experiment, we explored the parabolic trajectories of electron Airy beams (Fig. 1). We recorded profiles using an electron beam with a relatively large area (100 μm × 100 μm). Figure 1a shows the numerical (simulated using the beam propagation numerical method[21]) and the experimental transverse profiles of the diffracted electrons at several propagation distances behind the Fourier plane. The viewed diffracting orders are +1, −1, +2 and −2. As seen, Airy orders +1 and −1 anomalously converge in x and eventually collide, unlike the normal diffraction of Bragg peaks, which linearly diverge. As expected, the orders diverge in y. Unlike orders +1 and −1, orders +2 and −2 are almost constant in x and only slightly diverge in y. We traced the trajectories of the highest intensity lobe, of orders +1 and +2. The projections of the deflections of the orders into the x–z and y–z planes are shown in Fig. 1b. The values of $x(z)$ and $y(z)$ are given by pixel numbers, multiplied by 25 μm per pixel. The measured parabolic

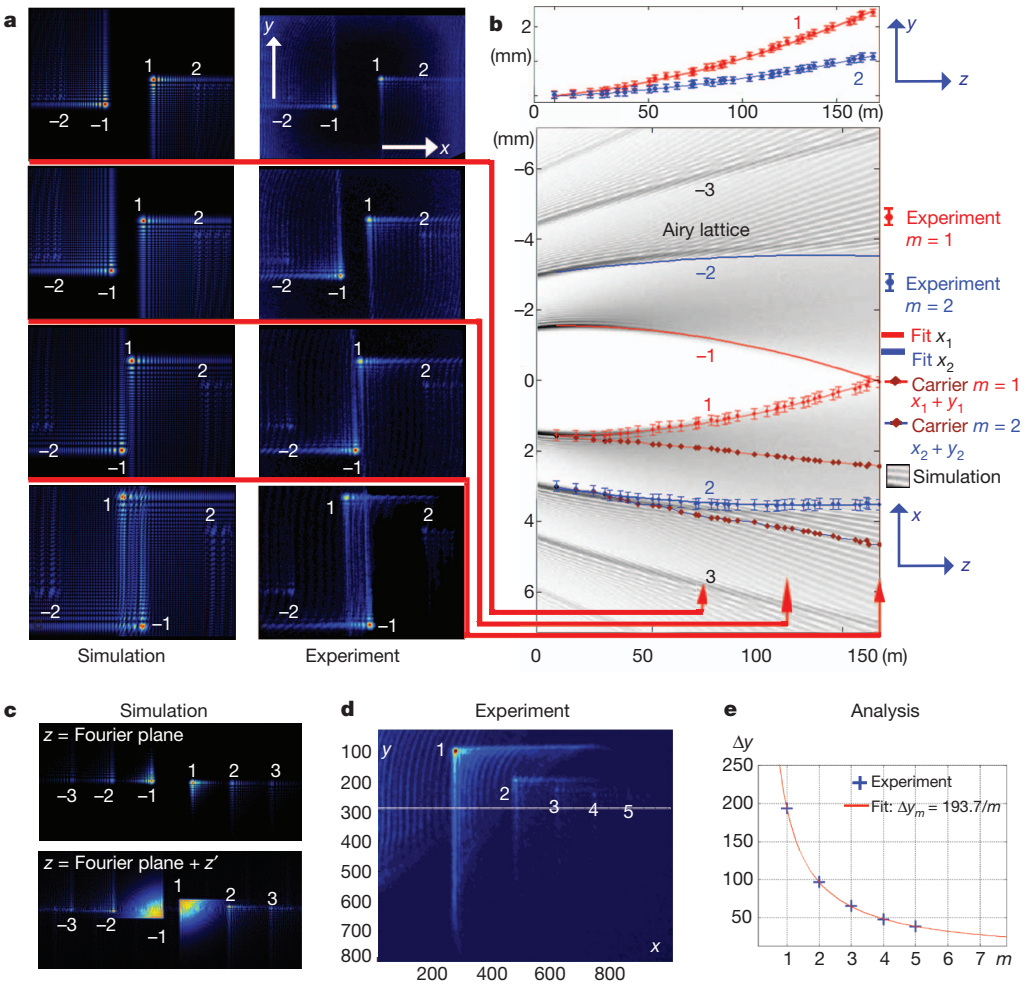

Figure 1 | Exploring the propagation dynamics of the Airy lattice. **a**, Comparison of micrographs of the transverse (x, y) profiles of the Airy lattice with simulation results, revealing the propagation dynamics of orders +1, −1, +2 and −2. **b**, The simulated trajectories of multiple Airy orders projected into the x–z plane versus the experimental results for orders +1 and +2 (y–z plane also shown). The error bars indicate the range of the estimated systematic error in the measurements. **c**, Propagation of the Airy lattice. **d**, Experimental micrograph revealing the first five Airy orders. **e**, The deflection in y of each order m is proportional to $1/m$.

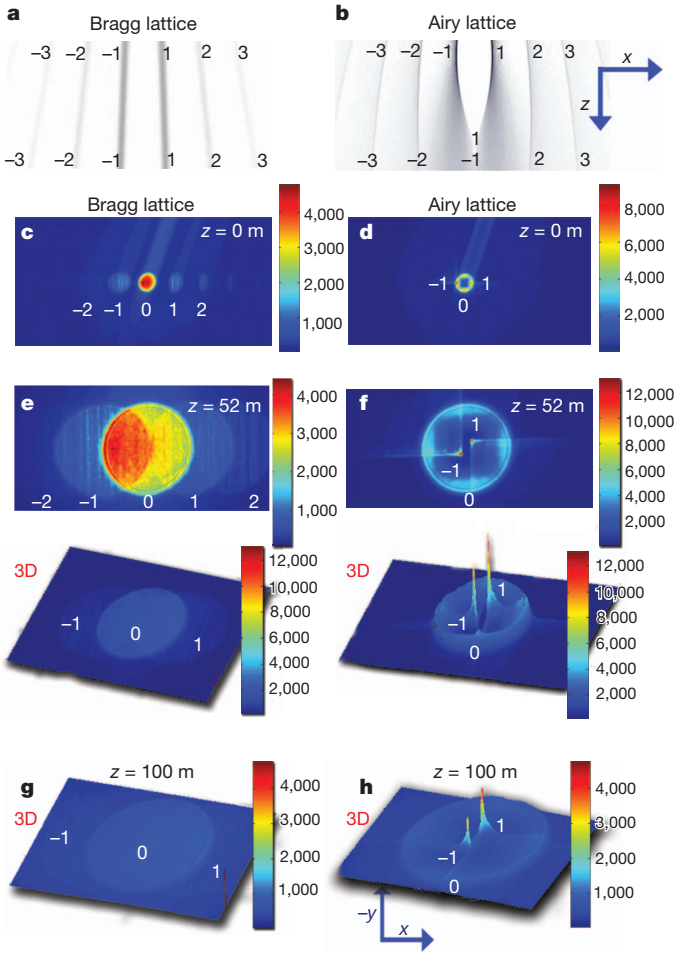

Figure 2 | Comparison between electrons diffracting from an Airy grating and the electrons diffracting from a reference periodic Bragg grating. **a**, The diffraction from a Bragg lattice is normally outward at an angle[9] $\alpha_m = m\lambda_B/\Lambda$. **b**, The diffraction from an Airy grating is anomalous because the lattice peaks are curved inward. **c**–**h**, Experimental profile micrographs of different propagation planes. Notice that the zeroth order looks the same in both the Airy lattice and the Bragg lattice. The Airy orders are very localized and maintain high intensities compared with the Bragg orders.

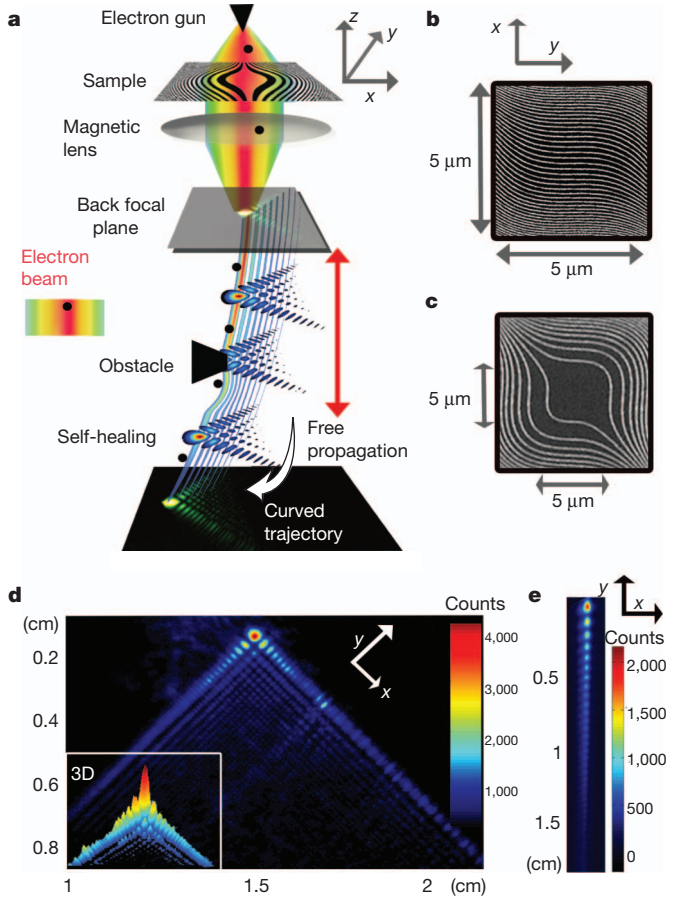

Figure 3 | Holographic generation of an electron Airy beam. **a**, An electron beam is transmitted through a nanofabricated hologram, with a cubic phase modulation. It is then focused by a magnetic lens. The Airy wave packet is formed at the back focal plane and recorded as it propagates. The electron Airy beam is a shape-preserving beam that evolves along a curved trajectory. It also self-heals after encountering obstacles. **b**, **c**, TEM micrographs of the nanoscale holograms: two-dimensional Airy on a spatial carrier frequency (**b**); two-dimensional Airy without a carrier (**c**). **d**, **e**, Experimental wave packet micrographs of two-dimensional (**d**) and one-dimensional (**e**) electron Airy beams.

trajectories are in the shape given by the analytical trajectories in equation (2). We note that the summation of the deflection of the carrier and the deflection in x is equal to the deflection in y. Also, the transverse linear coefficient increases by a factor of m, whereas the quadratic term decreases by a factor of $1/m$. This is why Airy beams of high order have almost linear trajectories like the Bragg peaks. This also explains the experimental results and the differences in propagation between orders 1 and -1 (which eventually collide in x) and orders 2 and -2. The fitting coefficients for the experimental results are presented in Table 1.

Another way to find the quadratic coefficient of the parabolic trajectory is by using only a single-profile picture at a fixed distance, z, from the Fourier plane (Fig. 1c–e). A single-profile picture reveals several Airy orders. Each Airy order diffracts with a different parabolic trajectory, having a different quadratic coefficient which is proportional to $1/m$. The deflection in y of each order in a single propagation plane (z has a fixed value) is $\Delta y = C_1/m$, where C_1 is a quadratic coefficient. This causes the Airy lattice to change its proportions. The diffraction orders that were located equidistantly in the Fourier plane, $z = 0$, diverge non-uniformly, and their proportions are not maintained (Fig. 1c and Supplementary Information, section 2). This is another demonstration of the parabolic propagation dynamics, which have been verified experimentally (Fig. 1d). The fitting curve of the experimental results presented in Fig. 1e is $\Delta y = 193.7/m$, matching the theoretical prediction. Detailed explanation of the parabolic trajectories measurement is given in Supplementary Information, sections 2 and 5. The collision between Airy beams represents a new way of interfering electron beams. The electron beam is separated into two diffraction orders, but these beams re-merge owing to their opposite directions (Fig. 1a, b). The measured deflection in x and y was 2.5 mm over an effective distance of 150 m.

We compared the electrons diffracting from an Airy grating with the electrons diffracting from a reference periodic Bragg grating. We simulated the evolution of electrons (Fig. 2a) diffracted from a periodic Bragg grating and from an Airy grating with the same carrier period. (Only in this case did we use different input beam areas for Airy and Bragg lattices, to visualize the trajectories.) As expected, the diffraction from a Bragg lattice is linear and outward; however, the diffraction

Table 1 | Quadratic fit results

Coefficient		C_1 (m^{-1})	C_2	C_3 (m)
$m = 1$	Δx	$-1.022e^{-7} \pm 1.51e^{-9}$	$7.141e^{-6} \pm 2.7e^{-7}$	$1.43e^{-3} \pm 4e^{-5}$
	Δy	$1.022e^{-7} \pm 1.51e^{-9}$	0	$-1.41e^{-4} \pm 2e^{-5}$
$m = 2$	Δx	$-4.869e^{-8} \pm 1.02e^{-9}$	$1.312e^{-5} \pm 2.7e^{-7}$	$2.68e^{-3} \pm 3.75e^{-5}$
	Δy	$4.869e^{-8} \pm 1.02e^{-9}$	0	$-8.59e^{-5} \pm 1.42e^{-5}$

Fits to Δx, $\Delta y = C_1 z^2 + C_2 z + C_3$ and 95% confidence intervals calculated from trough curve fitting.

Table 2 | Comparison between non-spreading Airy beams and spreading Bragg peaks

Propagation distance, z (m)	FWHM Bragg (μm)	FWHM Airy (μm)	FWHM Bragg/Airy
0	1,125	102	11
52	5,785	104	58
100	8,125	110	81

FWHMs of the diffracted beams.

from the Airy lattice is anomalously bent (inwards for low-index diffraction orders). In the second experiment, we recorded profiles (Fig. 2) using a relatively narrow input beam area (10 μm × 10 μm), letting the zero-order diffraction peak spread out to enable visualization of the difference between the evolution of spreading Bragg peaks and that of the shape-preserving Airy lattice peaks. The zeroth order of the Airy lattice is the only one that is not imprinted with a cubic phase; thus, it spreads in the normal manner. The zeroth order appears as a large circular spot in the middle of the frame. We can also see diffraction orders +1, −1, +2 and −2. At an effective distance of 100 m, the diffraction patterns from the Bragg lattice (as well as from the zeroth order of the Airy lattice) spread out linearly, become very large and decay in intensity. However, for $m \neq 0$ the curved Airy peaks stay confined to a very small area and maintain their high intensity. This difference is emphasized when calculating the full-widths at half-maximum (FWHMs) of the diffracted orders (Table 2).

We also measured the self-healing properties of electron Airy beams (Fig. 4). For this purpose, we used a glass wire placed in the diffraction plane. This wire is conventionally used as a bi-prism in electron holography[25], but in our case it was used simply to block parts of the beam. Increasing the current of the objective lens raised the Airy beam above the wire. Then we adjusted the wire to block Airy orders −1 and +1 simultaneously. We blocked the different orders in a slightly different manner. We then gradually increased the current of the diffraction lens and observed self-healing of the two orders[10]. The wave packets reconstructed their shapes after passing the blocking wire. As shown, the two orders self-healed differently. Order 1 self-healed faster than order −1. We also simulated the self-healing process and the numerical results are in a good agreement with the experimental results.

We have experimentally observed a non-spreading electron Airy wave packet whose highest-intensity quantum probability peaks bend in the absence of an external force. Our technique for generating electron Airy beams is analogous to the optical method[4], but makes use of recent advances in electron beam shaping[7] and nanoscale hologram fabrication techniques[8,9]. We measured the wave packet trajectories in two different ways. Our method of holographically generating

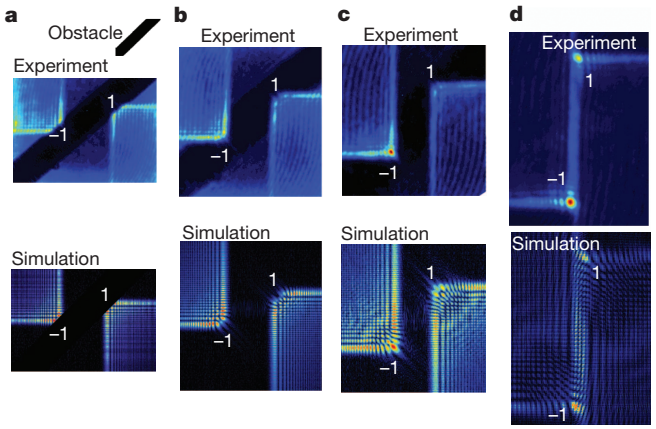

Figure 4 | Self-healing properties of electron Airy wave packets. **a–d**, Experimental profile photograph versus numerical simulation at different propagation planes after Fourier plane. The diffracted orders 1 and −1 are blocked differently and their self-healing processes are different. The two orders are blocked with a glass wire.

electron Airy beams suggests a general means of manipulating particles' wave packet trajectories by engineering their initial probability density wave functions. Our experimental results include demonstration of electron wave packet trajectories that show shape and size preservation over an effective length of more than 100 m. Such non-spreading Airy electron wave packets may be useful in improving the resolution properties of TEM imaging, because they have an extremely large depth of focus. Furthermore, we have shown that these electron wave packets self-heal and reconstruct their original shape after passing an obstacle. An interesting feature of these beams is that different diffraction orders with quadratic terms of opposite sign can be merged and possibly used as a new type of electron wave interferometer. The holographic generation of Airy electron beams can be generalized because recent studies have shown that optical Airy beams can be designed with arbitrary spatial shapes[5] and can propagate along arbitrary trajectories[6]. It may also be possible to use these beams to study electron spin–orbit interaction effects in the relativistic regime, similarly to recent studies of electron vortices[26]. Finally, there may be other ways of manipulating and shaping the trajectories and the self-healing properties of Airy beams, based on the ability to externally influence electrons using magnetic or electric potentials[27].

METHODS SUMMARY

Our analytical method of designing nanoscale holograms for electrons, imposed with any phase, is described in Supplementary Information, section 2. Our technique for determining the propagation dynamics of an electron beam, which we showed can be modelled numerically, is reported in Supplementary Information, section 5. We also developed a way of imaging electron wave packets with high magnification (Supplementary Information, section 4) and a way of manufacturing holographic masks for electrons with high writing resolution (Supplementary Information, section 3).

Received 2 August; accepted 4 December 2012.

1. Berry, M. V. & Balazs, N. L. Nonspreading wave packets. *Am. J. Phys.* **47,** 264–267 (1979).
2. Berry, M. & Upstill, C. *Catastrophe Optics: Morphologies of Caustics and their Diffraction Patterns* (Elsevier, 1980).
3. Airy, G. B. On the intensity of light in the neighbourhood of a caustic. *Trans. Camb. Phil. Soc.* **6,** 379–403 (1838).
4. Siviloglou, G. A., Broky, J., Dogariu, A. & Christodoulides, D. N. Observation of accelerating Airy beams. *Phys. Rev. Lett.* **99,** 213901 (2007).
5. Bandres, M. A. Accelerating parabolic beams. *Opt. Lett.* **33,** 1678–1680 (2008).
6. Greenfield, E., Segev, M., Walasik, W. & Raz, O. Accelerating light beams along arbitrary convex trajectories. *Phys. Rev. Lett.* **106,** 213902 (2011).
7. Uchida, M. & Tonomura, A. Generation of electron beams carrying orbital angular momentum. *Nature* **464,** 737–739 (2010).
8. Verbeeck, J., Tian, H. & Schattschneider, P. Production and application of electron vortex beams. *Nature* **467,** 301–304 (2010).
9. McMorran, B. J. *et al.* Electron vortex beams with high quanta of orbital angular momentum. *Science* **331,** 192–195 (2011).
10. Broky, J., Siviloglou, G. A., Aristide, D. & Christodoulides, D. N. Self-healing properties of optical Airy beams. *Opt. Express* **16,** 12880–12891 (2008).
11. Durnin, J. Miceli, J. J. & Eberly, J. H. Diffraction-free beams. *Phys. Rev. Lett.* **58,** 1499–1501 (1987).
12. Kaganovsky, Y. & Heyman, E. Wave analysis of Airy beams. *Opt. Express* **18,** 8440–8452 (2010).
13. Sztul, H. I. & Alfano, R. R. The Poynting vector and angular momentum of Airy beams. *Opt. Express* **16,** 9411–9416 (2008).
14. Baumgartl, J., Mazilu, M. & Dholakia, K. Optically mediated particle clearing using Airy wave packets. *Nature Photon.* **2,** 675–678 (2008).
15. Polynkin, P., Kolesik, M., Moloney, J., Siviloglou, G. A. & Christodoulides, D. N. Curved plasma channel generation using ultraintense Airy beams. *Science* **324,** 229–232 (2009).
16. Salandrino, A. & Christodoulides, D. N. Airy plasmon: a nondiffracting surface wave. *Opt. Lett.* **35,** 2082–2084 (2010).
17. Minovich, A. *et al.* Generation and near-field imaging of Airy surface plasmons. *Phys. Rev. Lett.* **107,** 116802 (2011).
18. Zhang, P. *et al.* Plasmonic Airy beams with dynamically controlled trajectories. *Opt. Lett.* **36,** 3191–3193 (2011).
19. Porat, G., Dolev, I., Barlev, O., &. Arie, A. Airy beam laser. *Opt. Lett.* **36,** 4119–4121 (2011).
20. Longhi, S. Airy beams from a microchip laser. *Opt. Lett.* **36,** 716–718 (2011).
21. Ellenbogen, T., Bloch, N. V., Ganany-Padowicz, A. & Arie, A. Nonlinear generation and manipulation of Airy beams. *Nature Photon.* **3,** 395–398 (2009).
22. Siviloglou, G. A., Broky, J., Dogariu, A. & Christodoulides, D. N. Ballistic dynamics of Airy beams. *Opt. Lett.* **33,** 207–209 (2008).

23. Dai, H. T., Sun, X. W., Luo, D. & Liu, Y. J. Airy beams generated by a binary phase element made of polymer-dispersed liquid crystals. *Opt. Express* **17,** 19365–19370 (2009).
24. Lee, W. H. Binary computer-generated holograms. *Appl. Opt.* **18,** 3661–3669 (1979).
25. Lichte, H. & Lehmann, M. Electron holography - basics and applications. *Rep. Prog. Phys.* **71,** 016102 (2008).
26. Bliokh, K. Y., Dennis, M. R. & Nori, F. Relativistic electron vortex beams: angular momentum and spin-orbit interaction. *Phys. Rev. Lett.* **107,** 174802 (2011).
27. Bliokh, K. Y., Bliokh, Y. P., Savel'ev, S. & Nori, F. Semiclassical dynamics of electron wave packet states with phase vortices. *Phys. Rev. Lett.* **99,** 190404 (2007).

Supplementary Information is available in the online version of the paper.

Acknowledgements N.V.-B. is an Eshkol scholar. This work was partly supported by the Israel Science Foundation and by the Israeli Ministry of Science. The author wishes to thank K. Shemer and D. Bloch for conversations.

Author Contributions N.V.-B. conceived the idea and designed the experiments. N.V.-B. and Y. Lereah carried out the experiment. Y. Lilach optimized the production process and fabricated the nanoscale holograms. A.G. and A.A. did the theoretical work and conceived ideas for applications. A.A. and N.V.-B. analysed the experimental results. A.G., A.A. and Y. Lereah provided experimental and theoretical guidance. A.A. and N.V.-B. developed and analysed the Airy lattice. All authors took part in writing the paper.

Author Information Reprints and permissions information is available at www.nature.com/reprints. The authors declare no competing financial interests. Readers are welcome to comment on the online version of the paper. Correspondence and requests for materials should be addressed to N.V.-B. (noavoloch@gmail.com).